Bio-Medical Materials and Engineering 27 (2016) 131–148
DOI 10.3233/BME-161573
IOS Press

Compound Doppler ultrasound signal simulation for pulsatile carotid arteries with a stenosis

Lian Gao [a], Yufeng Zhang [a,*], Yi Zhou [a], Xiao Hu [a], Li Deng [a], Kexin Zhang [b], Guanghui Cai [a] and Junhua Zhang [a]

[a] *Department of Electronic Engineering, Information School, Yunnan University, Kunming, Yunnan 650091, China*
E-mails: 962245641@qq.com, yfengzhang@yahoo.com, 3002380@qq.com, 1162019872@qq.com, 617674101@qq.com, ghcai@ynu.edu.cn, jhzhang@ynu.edu.cn

[b] *Cardiovascular Department, The Second Affiliated Hospital of Kunming Medical College, Kunming, Yunnan 650031, China*
E-mail: zhangkexingkm@vip.sina.com

Received 26 February 2015
Accepted 1 February 2016

Abstract.
BACKGROUND: The simulated Doppler blood flow signals are widely used to assess the performance of the clutter filters for removing wall components while reserving low-velocity signals scattered from physiological blood flow approaching the inner vessel-wall injured by a stenosed lesion.
OBJECTIVE: By simultaneously taking into account the natural attributes of the Doppler equipment, blood flow as well as vessel wall of pulsatile carotid arteries with a stenosis, a computer simulation method is presented to produce the compound Doppler ultrasound blood flow signals.
METHODS: The in-phase and quadrature (I/Q) axial as well as radial blood flow signals are simulated by superposing a series of cosine functions regulated by the spectrograms estimated from the axial and radial velocity profiles firstly obtained through the solution of the incompressible Navier–Stokes equations, respectively. Meanwhile, the I/Q Doppler signals echoed from pulsatile near (anterior) and far (posterior) walls are reproduced based on their radial movements during a cardiac cycle. Ultimately, those confirmed quadrature signals are summed to generate the compound Doppler signals including the contribution from both blood flow and stenosed vessel-wall.
RESULTS: The compound Doppler ultrasound signals echoed from both axial and radial blood flows as well as vessel walls with obstruction grades of 0% (normal arteries), 10% and 25% are simulated respectively. The real signals from the left carotid artery with an approximately 10% stenosis degree are also collected for further assessing the believability of simulated versions.
CONCLUSIONS: The simulated and clinical tests demonstrate that the proposed computer simulation method can produce compound Doppler signals with confirmed qualitative and quantitative characteristics resembled with the clinical versions, which could be used as an theoretical data source for evaluating the performance of the signal separation between pulsatile blood flows and vessel walls with mild stenosed-lesions.

Keywords: Compound Doppler signal simulation, physiological pulsation, carotid artery with a stenosis, axial and radial velocity profiles

*Corresponding author. E-mail: yfengzhang@yahoo.com.

1. Introduction

Stenosis is one of the most common arterial illnesses, which can confine the blood vessels, and may give rise to elevated blood flow velocity and shear stress, degressive or subtractive pressure at the narrowest position of stenosis, as well as decreasing shear stress, flow separation, wall contraction or even collapse at the downside of the stenosis [1,2]. These may be the fundamental reasons for thrombus generation and plaque cap fracture directly leading to heart attack and apoplexy [3]. Therefore, it is important to pay close attention to the early and correct identification of the risk factors affecting the stenosis formation and development for diagnosis of cardiovascular diseases.

Doppler ultrasound technique is a noninvasive, dynamic and easily accessible means widely adopted in diagnosis of cardiovascular diseases by assessing and quantifying the dynamic behaviours of blood vessel walls and the conditions of pulsatile blood flow. Some studies [4,5] have been carried out to acquire the acceleration as well as deceleration of blood vessel wall for noninvasively estimating the dynamic compliance of vascular substitutes as well as their pulsatile behaviour. It has been found that the obtained results can be used to reflect the degree of atherosclerotic changes in the vessel walls, which are benefit to conduct more detailed diagnosis of the arterial lesion.

While with the onset and development of cardiovascular lesions, the blood flow may be disarranged by atherosclerotic plaque attached to the inner membrane of vessel wall leading to the emergence of vortices or turbulence [6,7]. It seems reasonable to believe that more susceptive and exact inspection of the slight abnormal slowly-moving blood flow in proximity of the vessel wall could promote improvements in the diagnosis efficiency and medical outcomes. In recent years, a number of computational analysis and detection methods have been proposed to quantify blood flow distribution, involving that approaching the inner vessel-wall, to assess the wall shear rate (WSR) and the flow rate profiler (FRP) [8–13]. Because of the contamination of the low-frequency and great-amplitude clutters scattered from surrounding slowly-moving tissues (such as vessel walls), special clutter or wall filters for removing clutters from compound signals have been extensively researched [14–25]. In these studies, several wall removal approaches were presented, and their filtering performances were tested by employing compound Doppler signals achieved from either synthesis or simulation models.

The synthesis models [14–17] commonly employed the complex exponentials with a designated basic frequency and a corresponding phase shift superimposed by a random component with narrow band Gaussian distribution to synthesize mixed Doppler signals scattered from a random distribution of blood cells and the slowly-moving vessel wall passing through a sample volume. The synthesis models are limited to generate desirable simulation signals to test the capability of wall removing approaches because of insufficient consideration of the natural or physiologic attributes of the blood flow,artery walls as well as Doppler equipments. Several simulation approaches have been introduced [18–25] on account of the inherent features of blood flow, normal arteries (without stenosis) enclosed by the elastic tissue and ultrasound technique to produce compound Doppler signals. The composite simulated-signals present a similar form to those observed in Doppler instruments. The results also demonstrated that the simulation models ameliorated the believability and reality of compound simulation signals as they have controllable characteristics close to those obtained from clinical experiments. However, these simulation models mentioned above are restricted to produce the compound signals echoed from blood flow with only axial velocity component in healthy arteries. Therefore, it is necessary to simultaneously take into account the contribution of the both axial and radial blood flows due to the disturbance of the atherosclerotic plaque as well as pulsatile vessel walls when the study of the simulation mode is conducted to

achieve the compound Doppler ultrasound signals from pulsatile carotid arteries with a stenosed lesion.

The aim of this paper is to present a computer simulation method to produce compound Doppler ultrasound signals scattered simultaneously from both blood flow and vessel wall of pulsatile common carotid arteries. To simulate the full in-phase and quadrature (I/Q) blood flow signals, the radial blood flow velocity distribution under the stenosis condition is obtained by an extension study from previous researches on the Doppler signal simulation of the axial blood flow [26,27] by solving the NSEs in view of the center velocity of a normal vessel and geometric characteristics of the stenosed vessel, and then, the signals are simulated by superposing a series of cosine functions regulated by the spectrograms estimated from the axial and radial velocity profiles, respectively. Meanwhile, the I/Q Doppler signals echoed from pulsatile near and far walls (close to and far away the ultrasound probe, respectively) are reproduced based on their radial movements during a cardiac cycle. Ultimately, the confirmed quadrature signals incorporating the moving information backscattered from both axial and radial flows as well as pulsatile vessel walls are summed to generate the compound Doppler signals with regard to a definite sample volume. Both of the simulated and clinical trials are carried out to examine the performance of the introduced simulation method.

The rest of this paper is constructed as follows. Section 2 concentrates on a detail description of the method to simulate compound Doppler signals from axial and radial blood flows, as well as pulsatile vessel walls with the gentle regional-stenosis, respectively. Section 3 treats the simulation and clinical experiments for evaluating the performance of the presented simulation method. The last covers the results, discussions and conclusions.

2. Methods

2.1. The geometric shape of a stenotic artery

The stenotic artery can be described as a sine-shaped tube fraction with a radially and axially symmetrical circular cross section, which is displayed in Fig. 1 and delineated as

$$R(z) = \hat{R} - \frac{h}{2}\left(1 + \cos\frac{\pi z}{z_0}\right), \quad z \in [-z_0, z_0], \tag{1}$$

where $R(z)$ is the radius of sine-shaped arterial-fragment in the obstructed zone, $\hat{R}$ denotes the artery radius in the normal (unobstructed) region, h is the maximum height of the stenosis and $2z_0$ is the total axial distance of the obstruction.

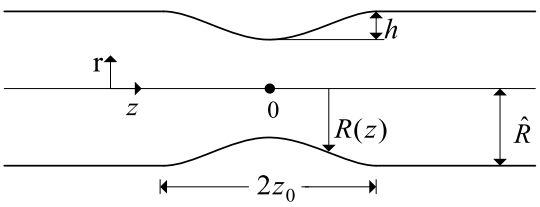

Fig. 1. The geometric model of the artery with a stenosed lesion.

2.2. Doppler ultrasound signal simulation for axial and radial blood flows

It is supposed that the pulsatile blood flow in the obstructed vessel fragment with a sine appearance is axisymmetrical, and exhibits the property of an incompressible Newtonian fluid. The momentum and continuity equations related to this pulsatile blood flow could be described by the linear NSEs [26] expressed as Eq. (2) under the cylindrical coordinate system where z stands for the longitudinal coordinate taking along the axis of the artery while r is the radial coordinate.

$$\begin{aligned}
&\frac{\partial V_a}{\partial z} + \frac{1}{r}\frac{\partial (r V_r)}{\partial r} = 0, \\
&\frac{\partial V_a}{\partial t} = -\frac{1}{\rho}\frac{\partial p}{\partial z} + \frac{\eta}{\rho}\left(\frac{\partial^2 V_a}{\partial r^2} + \frac{1}{r}\frac{\partial V_a}{\partial r}\right), \\
&\frac{\partial p}{\partial r} = 0,
\end{aligned} \tag{2}$$

where V_a and V_r denote the axial and radial velocities, respectively; p is the pressure, ρ and η denote the blood density and viscosity, respectively; t is time. The boundary states of the velocities on the vessel wall with mild stenosed-lesions are written as:

$$V_a|_{r=\hat{R}} = 0; \qquad V_r|_{r=\hat{R}} = 0 \tag{3}$$

and the conditions on the axis center is:

$$\frac{\partial V_a}{\partial r}\Big|_{r=0} = 0. \tag{4}$$

The relevant modulus (pressure, pressure gradient and velocities) could be expanded as complex Fourier series as follows due to the periodicity of blood flow:

$$\begin{aligned}
V_a &= V_{a_0} + \mathrm{Re}\left(\sum_{k=1}^{K} V_{a_k} e^{i\omega_k t}\right), \\
V_r &= V_{r_0} + \mathrm{Re}\left(\sum_{k=1}^{K} V_{r_k} e^{i\omega_k t}\right), \\
\frac{\partial p}{\partial z} &= P_{g_0} + \mathrm{Re}\left(\sum_{k=1}^{K} P_{g_k} e^{i\omega_k t}\right),
\end{aligned} \tag{5}$$

where Re() is a function to extract real parts of the complex quantity, $\omega_k = \omega k = \frac{2\pi}{T}k$ is angular frequency, T represents the cardiac cycle, and i is equal to $\sqrt{-1}$. By substituting the complex Fourier exponential form of the flow parameters presented in Eq. (5) into Eqs (2)–(4), and considering the linearity of Eq. (2) as well as homogeneity of Eqs (3)–(4), the axial ($V_a(y,t)$) and radial ($V_r(y,t)$)

velocity profiles of the pulsatile blood flow in arteries with the stenosis can then be obtained:

$$\begin{aligned}
V_a(y,t) &= \frac{\hat{R}^2}{4\eta}\left(y^2 - y_1^2\right)P_{g_0} + \mathrm{Re}\left(\sum_{k=1}^{K}\frac{\hat{R}^2}{i\eta\xi_k^2}\left[\frac{J_0(i^{3/2}\xi_k y)}{J_0(i^{3/2}\xi_k y_1)} - 1\right]P_{g_k}e^{i\omega_k t}\right),\\
V_r(y,t) &= \frac{\hat{R}^2 y}{14\eta}\left[4y_1 y_1' P_{g_0} + \left(2y_1^2 - y^2\right)\frac{dP_{g_0}}{dz}\right]\\
&\quad + \mathrm{Re}\left\{\sum_{k=1}^{K} -\frac{\hat{R}^3}{i\eta\xi_k^2}\left[\left(\frac{1}{i^{3/2}\xi_k}\frac{J_0(i^{3/2}\xi_k y)}{J_0(i^{3/2}\xi_k y_1)} - \frac{y}{2}\right)\frac{dP_{g_k}}{dz}\right.\right.\\
&\quad \left.\left. + \frac{J_1(i^{3/2}\xi_k y_1)J_1(i^{3/2}\xi_k y)}{J_0^2(i^{3/2}\xi_k y_1)}y_1' P_{g_k}\right]e^{i\omega_k t}\right\},
\end{aligned} \tag{6}$$

where $y = \frac{r}{\hat{R}}$, $y_1 = \frac{R(z)}{\hat{R}}$, $y_1' = \frac{dy_1(z)}{dz}$, $\xi_k = \hat{R}\sqrt{\frac{\rho\omega_k}{\eta}}$, $k = 1, 2, 3, \ldots$; J_0 and J_1 represent the first kind Bessel functions with zero and first orders, respectively. After that, the primary task is to determine the pressure gradient coefficients P_{g_0} and P_{g_k} in Eq. (6) for ultimately getting the axial ($V_a(y,t)$) and radial ($V_r(y,t)$) velocity profiles of pulsatile blood flow in the vessels with a stenosed lesion. Considering the boundary conditions of V_r on the vessel wall ($V_{r_0}|_{y=y_1} = 0$ and $V_{r_k}|_{y=y_1} = 0$), by substituting $y = y_1$ into the computing formula of $V_r(y,t)$, the following differential equations satisfied by P_{g_0} and P_{g_k} are derived:

$$\frac{dP_{g_0}}{dz} + \frac{4y_1'}{y_1}P_{g_0} = 0, \tag{7}$$

$$\frac{dP_{g_k}}{dz} + \frac{2y_1'}{y_1}\frac{J_1^2(i^{3/2}\xi_k y_1)}{J_0(i^{3/2}\xi_k y_1)J_2(i^{3/2}\xi_k y_1)}P_{g_k} = 0, \tag{8}$$

where J_2 denotes the first kind Bessel function with second order. Taking the solution of Eqs (7)–(8), P_{g_0} and P_{g_k} can then be achieved as:

$$P_{g_0} = P_{g_0}^*\frac{1}{y_1^4}, \tag{9}$$

$$P_{g_k} = P_{g_k}^*\frac{(i^{\frac{3}{2}}\xi_k)^2 J_0(i^{\frac{3}{2}}\xi_k) - 2i^{\frac{3}{2}}\xi_k J_0(i^{\frac{3}{2}}\xi_k)}{J_0(i^{\frac{3}{2}}\xi_k)}\frac{J_0(i^{\frac{3}{2}}\xi_k y_1)}{(i^{\frac{3}{2}}\xi_k y_1)^2 J_0(i^{\frac{3}{2}}\xi_k y_1) - 2i^{\frac{3}{2}}\xi_k y_1 J_1(i^{\frac{3}{2}}\xi_k y_1)}, \tag{10}$$

where $P_{g_0}^* = -\frac{4\eta V_{a_0}^*}{\hat{R}^2}$ and $P_{g_k}^* = i\eta\xi_k^2 V_{a_k}^*/\{\hat{R}^2[\frac{1}{J_0(i^{3/2}\xi_k)} - 1]\}$ are confirmed by the Fourier-expansion coefficients ($V_{a_0}^*$ and $V_{a_k}^*$) of the symmetry axis ($y = 0$) velocity $V_a(z^*, 0, t)$ in the stenosed section upwards at determined location (where $z = z^* = -5\hat{R}$, $R(z^*) = \hat{R}$ and $y_1 = 1$), which is obtained previously by a Doppler ultrasound system.

Based on the axial and radial velocity profiles determined by Eq. (6), the corresponding theoretical blood flow spectrograms can be reckoned by employing the overall-distribution nonparametric estimation (ODNE) method [28] in which the power spectral density (PSD) of the Doppler blood signals

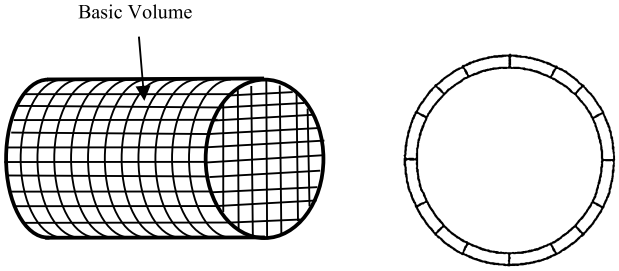

Fig. 2. The division of the vessel lumen for the blood flow spectrogram calculation (the left) and the vessel wall for the simulation of the Doppler signal from the wall motion (the right).

comprises the contributions of all blood cells flowing through the sample volume (SV), which is separated into a series of basic volumes (BVs) in the axial and radial directions, respectively. The separation of the SV for estimating the theoretical spectrograms is displayed in the left of Fig. 2.

Ultimately, the cosine-superposed method proposed by Mo [29] is employed to generate the complex quadrature axial ($S_{b_a}(t)$) as well as radial ($S_{b_r}(t)$) Doppler blood flow signal according to their corresponding theoretical spectrograms:

$$S(t) \approx \sum_{m=1}^{M} \gamma_m \exp\left[i(2\pi f_m t + \varphi_m)\right], \tag{11}$$

where $f_m = (m - \frac{1}{2})\Delta f$, $\gamma_m = \sqrt{2T_s(t, f_m)\Delta f \zeta_m}$, $\Delta f = f_{\max}/N_1$, $N_1 = 2f_{\max}T$, T denotes the signal duration time. φ_m is the stochastic phase, which is distributed uniformly over $[0, 2\pi]$, ζ_m denotes a χ-squared random variable having two degree of freedom (χ_2^2), $T_s(t, f_m)$ represents the theoretical spectrograms determined by the time varying PSDs and $f_{\max}$ is its maximum frequency at this position. γ_m is the amplitudes of the complex exponential functions obeyed Rayleigh distributed, and M is the number of complex exponential functions confirmed by the maximum frequency $f_{\max}$ and signal duration time T.

2.3. Doppler ultrasound signal simulation for pulsing vessel walls

In order to carry blood from heart to all parts of the human body, the cross-section area of the artery alters with blood pressure during the cardiac cycle. Due to the elastic feature of the vessel walls composed of monolayer cell and basement membrane, the near and far walls can be found to be expanded outwardly to maximum vessel diameter during the systole and rebounded slowly to the normal conditions during the final phase of diastole. The radial pulse of vessel wall also brings the frequency variation in Doppler ultrasound signals. The phase adaption related to the slowly-pulsing near and far nonlinear elasticity vessel walls can be written respectively as [25]:

$$\begin{aligned} \varphi_n(t) &= 4\pi \frac{\gamma_n(t) f_0}{c}, \\ \varphi_f(t) &= 4\pi \frac{\gamma_f(t) f_0}{c}, \end{aligned} \tag{12}$$

where $\gamma_n(t)$ and $\gamma_f(t)$ denotes the radial displacements of the near and far vessel walls, respectively; f_0 is the ultrasound-emitting frequency and c represents the mean velocity of ultrasound in tissue. So

the antecedent and posterior vessel wall Doppler signal can be achieved respectively as:

$$\begin{aligned} S_{nw1}(t) &= \alpha_{nw} \exp\big(j\varphi_n(t)\big), \\ S_{fw1}(t) &= \alpha_{fw} \exp\big(j\varphi_f(t)\big), \end{aligned} \tag{13}$$

where α_{nw} and α_{fw} denote the amplitude constants of the antecedent and posticus wall constituents, respectively.

The appropriate division of the vessel wall in the SV into a series of BVs along the ring-shaped circumference is carried out and displayed in the right of Fig. 2. Then the entire wall signal, $S_w(t) = S_{nw1}(t) + S_{fw1}(t)$, can be reproduced by summation of the contributions from all sub-sampling volumes calculated by Eq. (13).

2.4. The composition of the blood and wall signals

The I/Q Doppler ultrasound signals including the moving information backscattered from both axial and radial blood flows as well as vessel walls of pulsatile stenosed-common carotid arteries are achieved by summing the obtained blood flow and vessel wall signals with respect to the determined sample volume by:

$$S_c(t) = S_b(t) + S_w(t) \tag{14}$$

with a ratio of the I/Q wall to blood (IQWBR) signals:

$$\text{IQWBR} = 20 \log 10 \frac{|S_w(t)|}{|S_b(t)|}, \tag{15}$$

where $S_b(t)$ is the full Doppler blood flow signals including the axial component $S_{b_a}(t)$ and radial component $S_{b_r}(t)$ simulated by Eq. (11) at ultrasound incident angle θ as:

$$S_b(t) = S_{b_a}(t) \sin\theta + S_{b_r}(t) \cos\theta. \tag{16}$$

3. Experiments

To assess the performance of the presented simulation method, compound quadrature-Doppler ultrasound signals from the pulsatile axial as well as radial blood flow and vessel walls with various stenosis grades of 0% (normal arteries), 10% and 25% in the SV axially ranging from $z = 0\hat{R}$ (the inlet of the stenosis) to $4\hat{R}$ (the outlet of the stenosis) are reproduced by the approach described in detail above. The characteristic factors are employed to tightly correspond with those using in commercial Doppler ultrasound equipment, and enumerated as: the artery radius in the unobstructed region $\hat{R} = 5$ mm, the axial length of the stenosis segment $2z_0 = 8\hat{R}$, blood density $\rho = 1050\,\text{kg/m}^3$, blood viscosity $\eta = 3.5 \times 10^{-3}$ Pa $\cdot$ s, cardiac cycle $T = 1$ s, the quantity of Fourier series expansion equation $K = 14$, the ultrasound-emitting frequency $f_0 = 5$ MHz, the ultrasound velocity $c = 1540$ m/s, and the ultrasound incident angle $\theta = 30°$. By using a $100 * 100$ Cartesian grid, the SV of the vessel lumen with 20 mm obstruction length is separated into 120 coordinate components along the vessel axis and 50 circle rings with equivalent thickness along the radius. At the same time, the division of the vessel wall into 100 coordinate components known as the ring-shaped circumference is implemented.

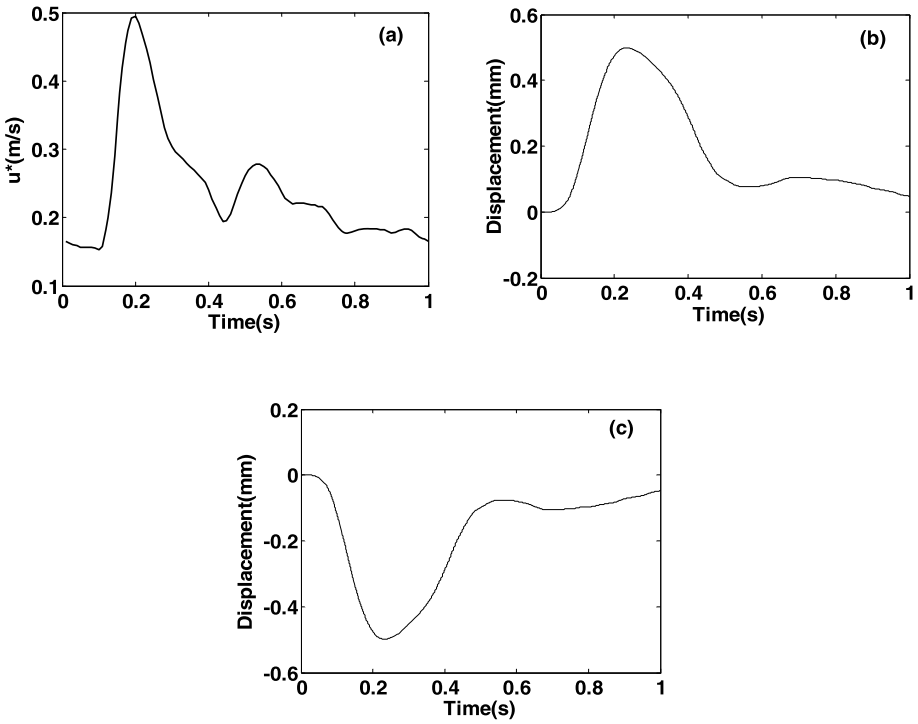

Fig. 3. The waveforms of the axial centerline velocity waveform $V_a(z^*, 0, t)$ (a), the near wall displacement $\gamma_n(t)$ (b) and the far wall displacement $\gamma_f(t)$ (c).

In the experimental study, I/Q Doppler blood signals scattered from pulsatile axial and radial blood flow in the healthy vessel and stenosed vessels with obstruction grades of 10% and 25% axially located in $z = 0\hat{R}$ to $4\hat{R}$ downstream of the throat of the stenosis are firstly simulated by Eq. (11). In this trial, the spectrogram $T_s(t, f_m)$ in Eq. (11) is estimated from corresponding velocity profiles obtained by solving Eqs (2)–(10) based on the symmetry axis ($y = 0$) velocity distribution $V_a(z^*, 0, t)$ in the stenotic vessel section upwards at determined location ($z = z^* = -5\hat{R}$, $R(z^*) = \hat{R}$ and $y_1 = 1$) displayed in Fig. 3(a). Meanwhile, the I/Q Doppler signals echoed from the near and far walls are generated by using Eqs (12)–(13) with the input waveforms of the radial displacements of the antecedent ($\gamma_n(t)$) and posticus ($\gamma_f(t)$) vessel walls shown in Fig. 3(b) and (c), respectively. Finally, compound Doppler ultrasound signal with an IQWBR of 20 dB are achieved by using Eqs (14)–(16). To evaluate the simulation performance, the time-varying spectrograms of all simulated I/Q signals are estimated by employing a short time Fourier transform (STFT) with a 10 ms temporal window for evaluation. For further quantificationally evaluating the validity of simulated compound-signals, a calculation based on 30 realizations is carried out to achieve the mean and standard deviation (MSD) of the normalized root-mean-square deviation among the theoretical and ensemble-averaged time-varying spectrograms (NRMSESs) of compound Doppler ultrasound signals from 30 simulations by:

$$\text{NRMSESs} = \frac{\sqrt{\sum_{m=0}^{M-1}(S(m) - \overline{S}(m))^2}}{\sqrt{\sum_{m=0}^{M-1}(\overline{S}(m))^2}}, \tag{17}$$

where $\overline{S}$ is the theoretical time-varying spectrogram and S represents the averaged version with the length M for the 30 simulated signals.

For further assessment of the proposed simulation method,the real signals from the left carotid artery with an approximately 10% stenosis degree determined previously by the CT and MRI are also collected in accordance with the ethical standards of the responsible committee on human experimentation. The compound I/Q Doppler ultrasound signals are firstly obtained from the determined male patient aged 55 years by using the continuous-wave Doppler blood flow detection instruments (VersaLab, Nicolet vascular Incorporated, CO, USA) with a 8 MHz transducer. The traditional vessel wall filter known as HPF is shut off to obtain the quadrature analog demodulation signals scattered from the pulsatile carotid arteries including both the blood flow and vessel wall. Then the corresponding digitized signals can be obtained by using an external sound blaster with two sampling channels inserted into a conveyable PC by an USB interface. The 22.5 MHz sample rate and 16 bit word length are used in digitization. The STFT-based spectrograms of the compound real signals and the signals extracted by using the HPF with cut-off frequency of 400 Hz (100 Hz intervals) are respectively achieved based on the same methods employed in the simulation experiments. The STFT-based spectrograms and spectra obtained from the real signals are compared with those derived in the simulation cases. All of the simulation and comparative experiments are implemented in Matlab 7.8 (The Mathworks, Inc., Natick, MA, USA).

4. Results

As shown in Fig. 4(a)–(c), the velocity profiles of axial blood flow for the healthy artery (Fig. 4(a)) and artery with obstruction grades of 10% (Fig. 4(b)) and 25% (Fig. 4(c)) are respectively achieved according to Eq. (6) based on the symmetry axis ($y = 0$) determined velocity $V_a(z^*, 0, t)$ exhibited in Fig. 3(a). For the stenosis cases shown in Fig. 4(b)–(c), similar variation characteristics of axial velocity distributions to those for the normal artery (Fig. 4(a)) can be found except that the maximum velocities of blood flow during systole as well as velocities of the tardy blood flow approaching the stenosed arterial walls are proportionately enlarged with the raise of the stenosis grades.

The theoretical spectrograms of the axial blood flow in the SV with extent 20 mm centered on $z = 2\hat{R}$ in the artery with stenosis grades of 0% (healthy artery), 10% and 25% are calculated by employing the ODNE method, and exhibited in Fig. 4(d)–(f), respectively. It is worth noting that during the entire carotid cycle, the pulsatile modes of the spectrograms for the axial blood flows in both healthy (Fig. 4(d)) and obstructed arteries (Fig. 4(e) for 10% and Fig. 4(f) for 25%) are similar to their own velocity profiles'. The frequency shifts raise fleetly and come up to its crest when time t approaches to 0.2 s. By comparing the experiment outcomes displayed in Fig. 4(d)–(f), the bandwidth and maximum frequency are proportionately enlarged whereas the spectral window reduced with the raise of the stenosis grades. However, the variations mentioned above for the 10% obstructed artery (Fig. 4(e)) are less than those for the 25% obstructed one.

Figure 4(g)–(l) show the in-phase (Fig. 4(g)–(i)) and quadrature (Fig. 4(j)–(l)) simulated Doppler signals echoed from axial blood flow in the artery with different obstruction grades of 0% (Fig. 4(g) and (j)), 10% (Fig. 4(h) and (k)) and 25% (Fig. 4(i) and (l)). All of them are stochastic allocation reflecting the time-varying nonstationary characteristic of axial blood flow and their distinctions are undoubtedly hard to be achieved. In order to evaluate their validities, their time-varying spectrograms are calculated by employing STFT with a 10 ms temporal window and exhibited in Fig. 4(m)–(o). The results show that STFT-based spectrograms present high consistencies with the corresponding theoretical versions

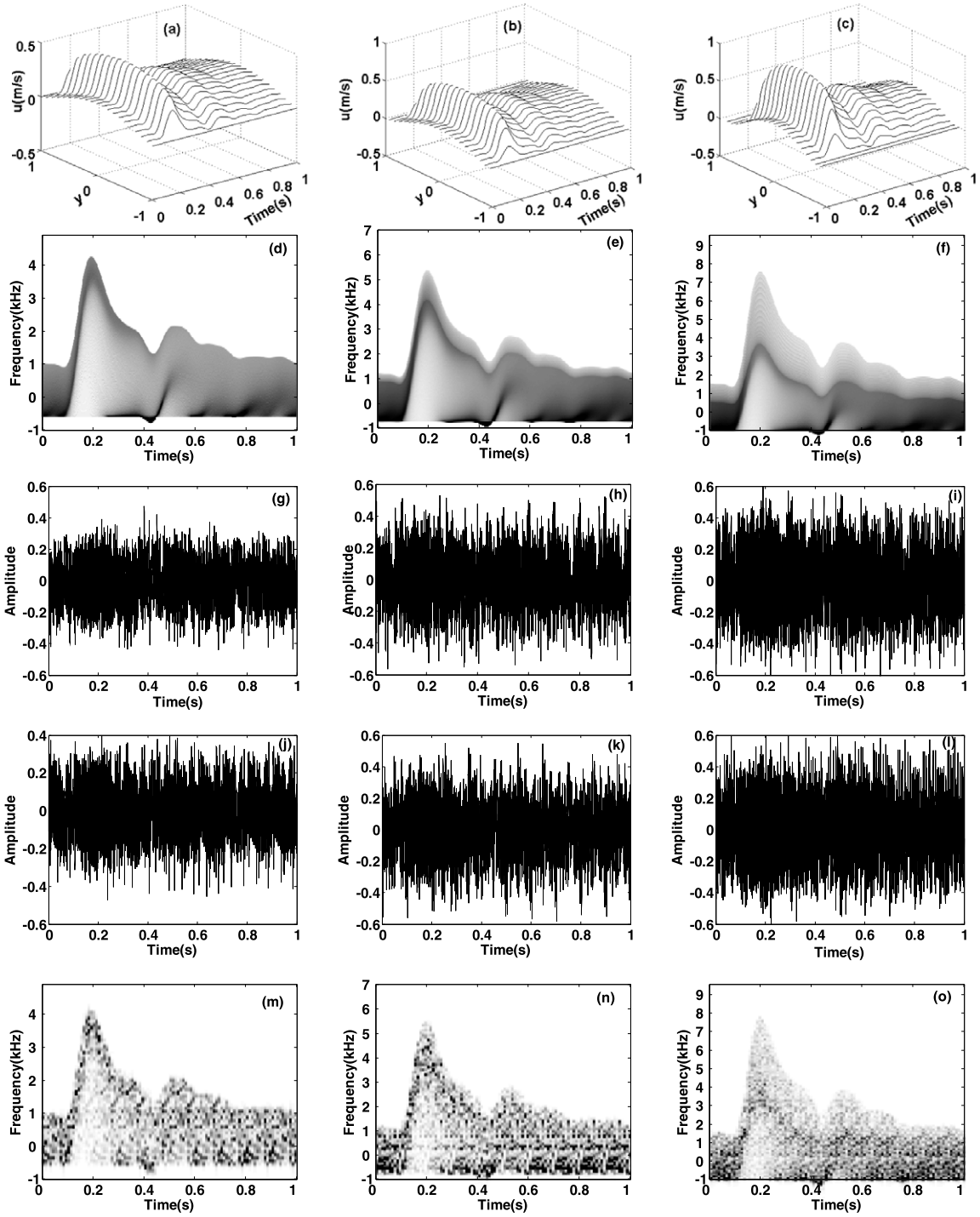

Fig. 4. The velocity distributions (a)–(c), theoretical spectrograms (d)–(f), the simulated in-phase (g)–(i) and quadrature (j)–(l) Doppler signals, and their STFT spectrograms (m)–(o) of the *axial blood flow* signals in the normal vessel ((a), (d), (g), (j), (m)) and vessel with obstruction grades of 10% ((b), (e), (h), (k), (n)) and 25% ((c), (f), (i), (l), (o)) over the axial range from $z = 0\hat{R}$ to $4\hat{R}$.

(Fig. 4(d)–(f)). In addition, the Doppler speckles emerging in the STFT-based spectrograms have a considerable similarity with those observed in sonographies of actual Doppler blood flow signals in clinic.

Figure 5 shows the velocity profiles (Fig. 5(a)–(c)), the theoretical spectrograms (Fig. 5(d)–(f)), the in-phase (Fig. 5(g)–(i)) and quadrature (Fig. 5(j)–(l)) waveforms as well as their STFT-based spectrograms (Fig. 5(m)–(o)) of the simulated Doppler signals from radial blood flow in the healthy artery (Fig. 5(a), (d), (g), (j) and (m)) and arteries with stenosis grades of 10% (Fig. 5(b), (e), (h), (k) and (n)) and 25% (Fig. 5(c), (f), (i), (l) and (o)). Figure 5(a) indicates that the velocity of radial blood flow in normal vessel is zero everywhere at any point as the blood flows in normal vessels are laminar without radial components. Thus, the corresponding theoretical spectrogram (Fig. 5(d)), simulated I/Q Doppler signals (Fig. 5(g) and (j)) as well as the STFT-based spectrogram (Fig. 5(m)) are null. These results for radial blood flow in the healthy artery are coincided with clinical findings of laminar blood flow in healthy vessels [7].

But the axially antisymmetrical velocity profiles of radial blood flow in the arteries with obstruction grades of 10% and 25% are apparent as shown in Fig. 5(b)–(c). These can be attributed to that the blood flows in the stenosed vessel are disarranged by atherosclerotic plaques resulting in the appearance of vortices or turbulence with radial components. For a certain time, the absolute velocities in stenosis vessels (Fig. 5(b)–(c)) reach their maximums at radial locations of $y = \pm 0.75$, and then decreases slowly along the radial directions. They attain to zero smoothly at the lumen center ($y = 0$) while rapidly drop to zero on the vessel walls ($y = \pm 1$). At different radial positions away from the axis ($y \neq 0$), the radial blood flow velocities present the pulsatile variations during one cardiac cycle, in which the maximum velocities increases with the expansion of the stenosis grades. Special attention should be paid on that the radial velocities (Fig. 5(b)–(c)) are significantly smaller than the axial versions (Fig. 4(b)–(c)) at arbitrary radial positions for any occasions. These results considerably correlate to the physical and physiological characteristics of real signals received from clinic trials. The theoretical spectrograms of the radial blood flow in stenosed vessels (Fig. 5(e)–(f)) are symmetry about zero-frequency-axis, which are coincided with the axial antisymmetry velocity profiles. The negative-frequency components in the spectrograms are contributed from blood cells relatively moving away from the probe. In addition, the bandwidths and maximum frequencies of spectrograms also enlarge while the spectral window widths decrease with the increase of stenosis grades. Based on the theoretical spectrogram, the I/Q Doppler signals of radial blood flows in the 10% and 25% stenosed vessels are simulated, and shown in Fig. 5(h)–(i) and (k)–(l), respectively. It can be observed that signal amplitudes for the 25% stenosis vary faster than those from 10% stenosis artery. This observation is tally with the signals' frequency distribution.

Figure 6 shows the simulated I/Q Doppler ultrasound signals scattered from the near and far pulsatile vessel walls as well as its STFT-based spectrogram. Compared with the axial (Fig. 4(g)–(l)) and radial (Fig. 5(g)–(l)) Doppler blood flow signals, the wall signals characterize relatively greater amplitude, lower frequency shift, and coexistence of the positive as well as negative frequency components as they are scattered from the slowly bi-direction pulsing vessel walls, which are more powerful Doppler ultrasound reflector than the blood flow suspension scattered-particles.

The results of the compound Doppler ultrasound signals echoed from both axial and radial blood flows as well as vessel walls of pulsatile carotid arteries with stenosis grades of 0%, 10% and 25% over the axial range from $z = 0\hat{R}$ to $4\hat{R}$ are displayed in Fig. 7, in which subgraphs (a)–(f) are in-phase ((a)–(c)) as well as quadrature ((d)–(f)) Doppler signals and (g)–(i) are their STFT-based spectrograms. The contamination from vessel walls to the lower frequency blood flow signals can be shown clearly in time (Fig. 7(a)–(f)) as well as time-frequency domain (Fig. 7(g)–(i)). These results typically demonstrate that the simulated compound signals present the agreeable features with those obtained from clinical trials

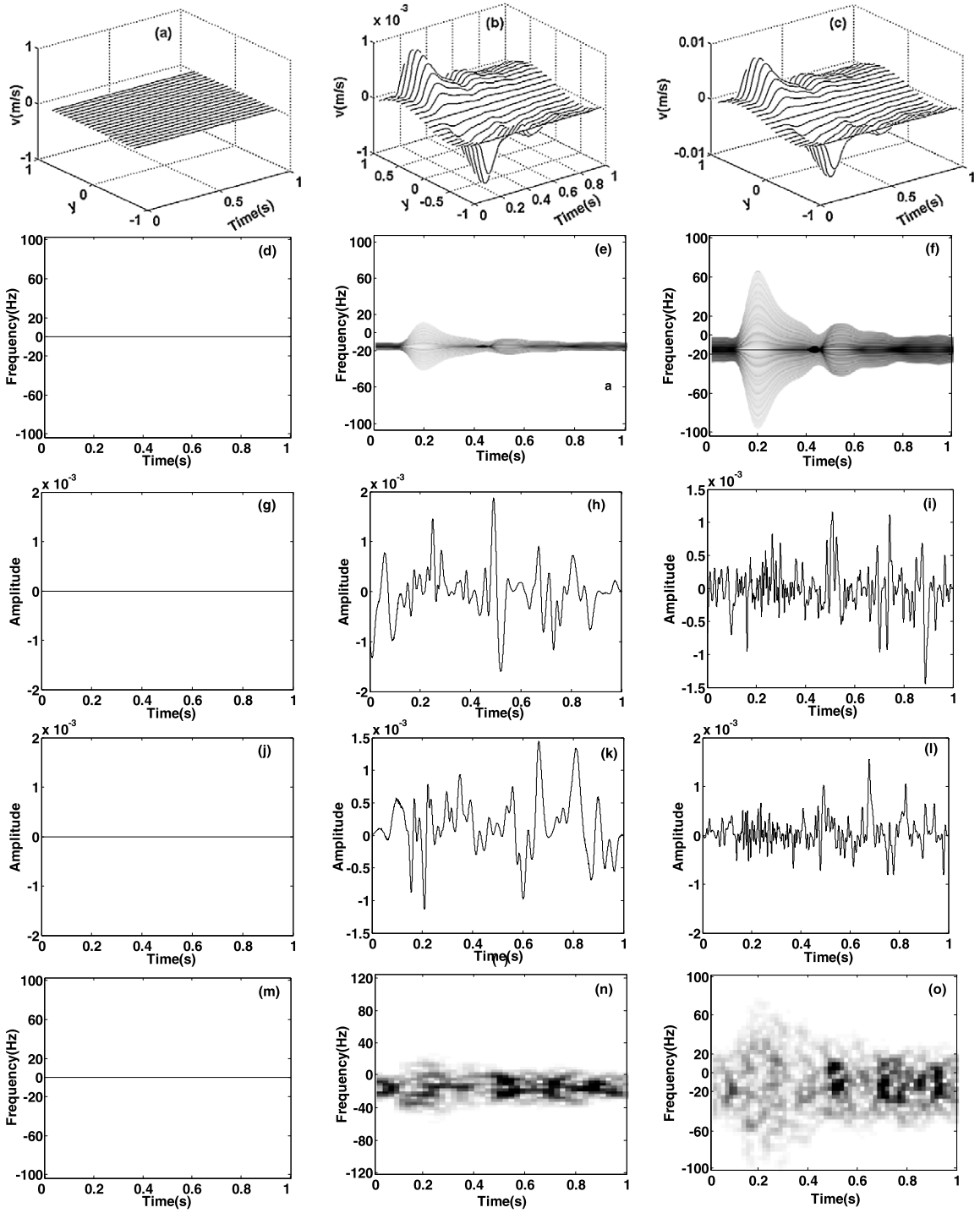

Fig. 5. The velocity distributions (a)–(c), theoretical spectrograms (d)–(f), the simulated in-phase (g)–(i) and quadrature (j)–(l) Doppler signals, and their STFT spectrograms (m)–(o) of the *radial blood flow* signals in the normal vessel ((a), (d), (g), (j), (m)) and vessel with obstruction grades of 10% ((b), (e), (h), (k), (n)) and 25% ((c), (f), (i), (l), (o)) over the axial range from $z = 0\hat{R}$ to $4\hat{R}$.

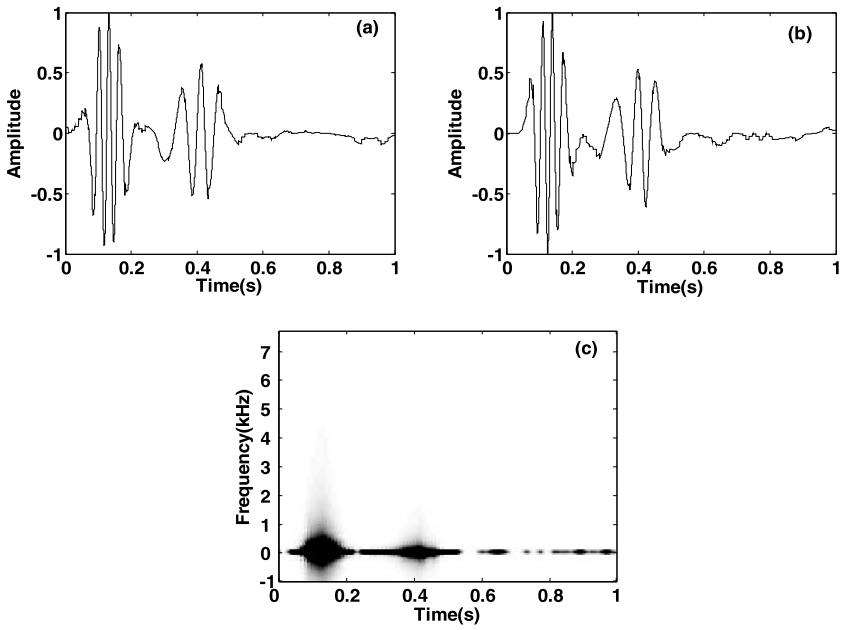

Fig. 6. The in-phase (a), quadrature (b) simulated-Doppler signal from the vessel wall and its STFT-based spectrogram (c).

(Fig. 8). The calculated MSD of NRMSESs from 30 realizations are 0.060 ± 0.003, 0.070 ± 0.001 and 0.041 ± 0.005 between the theoretical and averaged STFT-based spectrograms for 30 simulated compound Doppler ultrasound signals from arteries with stenosis grades of 0%, 10% and 25%, respectively. The quantificational NRMSESs reported above demonstrate the validation of the proposed computer simulation method.

For the sake of comparison study, compound Doppler ultrasound signals from a carotid artery with an approximate 10% stenosis degree are detected by using the continuous-wave Doppler blood flow detection instruments with a 8 MHz transducer by shutting down the wall filter. Figure 8 reports the in-phase (solid curves) and quadrature (dashed curves) time-domain waveforms (Fig. 8(a)) of the real I/Q compound signal, the STFT-based compound-spectrogram (Fig. 8(b)), as well as the blood flow- (Fig. 8(c)) and wall-spectrograms (Fig. 8(d)) separated by using a HPF with 400 Hz cut-off frequency. Figure 8(b) indicates that the contamination from the stenosed carotid artery walls is so considerably strong that it is hard to extract diagnostic features from the blood flow signal, especially that in the region approaching vessel walls for diagnosis of stenosis diseases. After the low-frequency components in the compound signal are filtered out, the major blood flow-spectrogram (Fig. 8(c)) presents the similar characteristics to those found from simulated axial-versions in Fig. 4(n), such as a rapid upstroke during the systolic period, a quick descent within early diastole, a slight oscillation during the late diastole and so on. At the same time, the wall-spectrogram shown in Fig. 8(d) also presents better consistency with the simulated version shown in Fig. 6(c), which demonstrates that the proposed computer simulation method can produce compound Doppler signals sharing similar characteristics with the clinical versions.

5. Discussion

In order to obtain a data source to evaluate the performance of the clutter or wall filters for removing clutters from compound blood signals, a set of synthesis [14–17] or simulation models [18–25] have

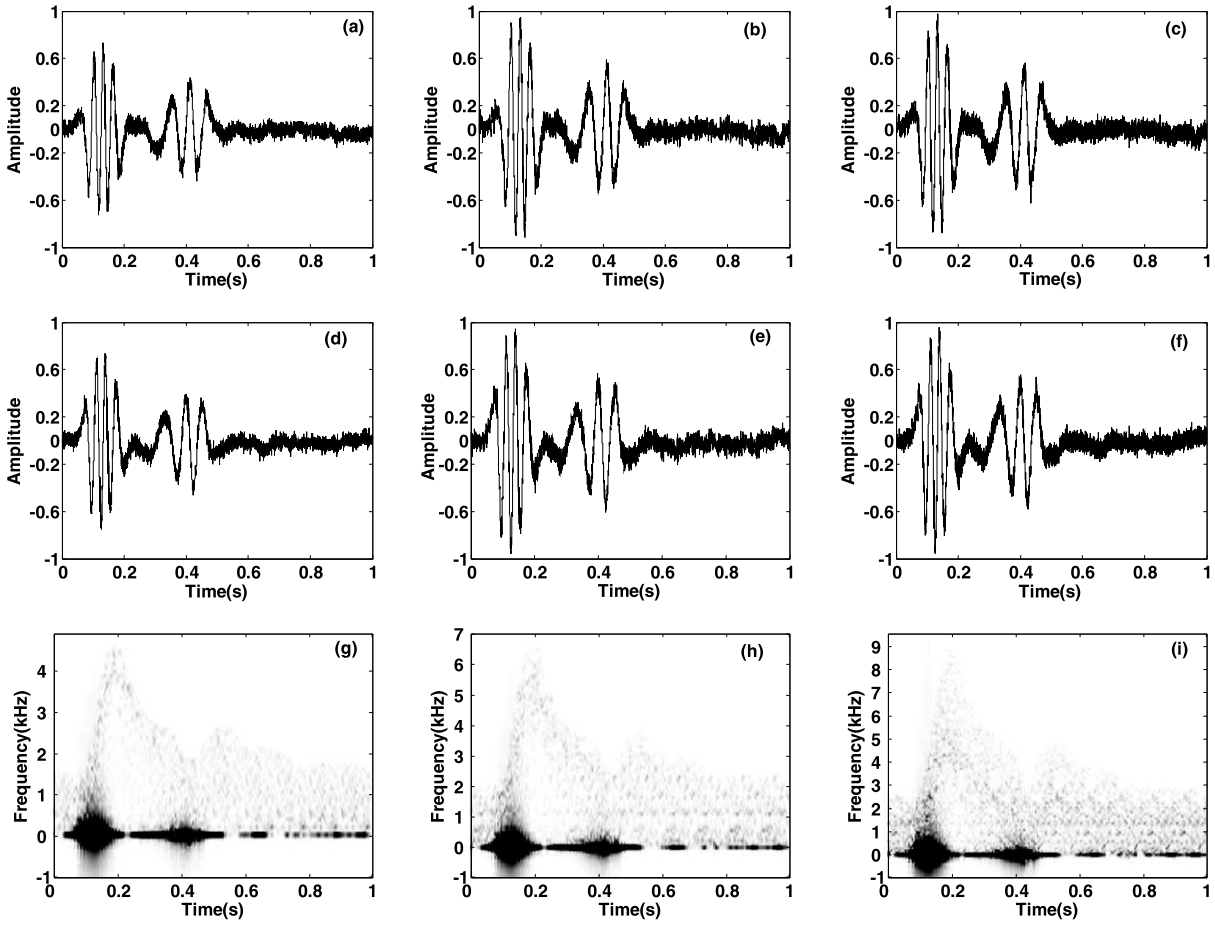

Fig. 7. The simulated I/Q compound Doppler signals (the in-phase component (a)–(c), the quadrature component (d)–(f)), and their STFT-based spectrograms (g)–(i) involving the motions backscattered from both axial and radial blood flows as well as the vessel walls of pulsatile normal artery ((a), (d), (g)) and artery with stenosis degrees of 10% ((b), (e), (h)) and 25% ((c), (f), (i)).

been proposed in recent years. Compared with the synthesis models, these simulation versions could produce more credible compound signals, while they were limited to pulsatile normal-vessels in which only axial blood flow exists. In an effort to advance the previously published simulation model, a method is proposed in this work to produce compound Doppler ultrasound signals including the contribution of the both axial and radial blood flows as well as pulsatile stenosed-common carotid walls. Although the geometric shape of the atherosclerotic plaque is theoretically simplified as the sinusoidal shape with a radially and axially symmetrical characteristic, it results in the alteration of the velocity profiles of axial blood flow and the emergence of the non-zero radial velocity-components at the region near the vessel walls. The simulated compound signals under these comprehensive conditions could a more objective data source for evaluating the performance of the signal separation between pulsatile blood flows and vessel walls with mild stenosed-lesions to a certain degree.

According to a set of results about the calculated velocity profiles (Figs 4 and 5(a)–(c)) based on the solution of the Navier–Stokes equations, as well as their theoretical spectrograms (Figs 4 and 5(d)–(f)) of axial (Fig. 4) and radial (Fig. 5) pulsatile blood flows, it is clear that the blood flow state tends to

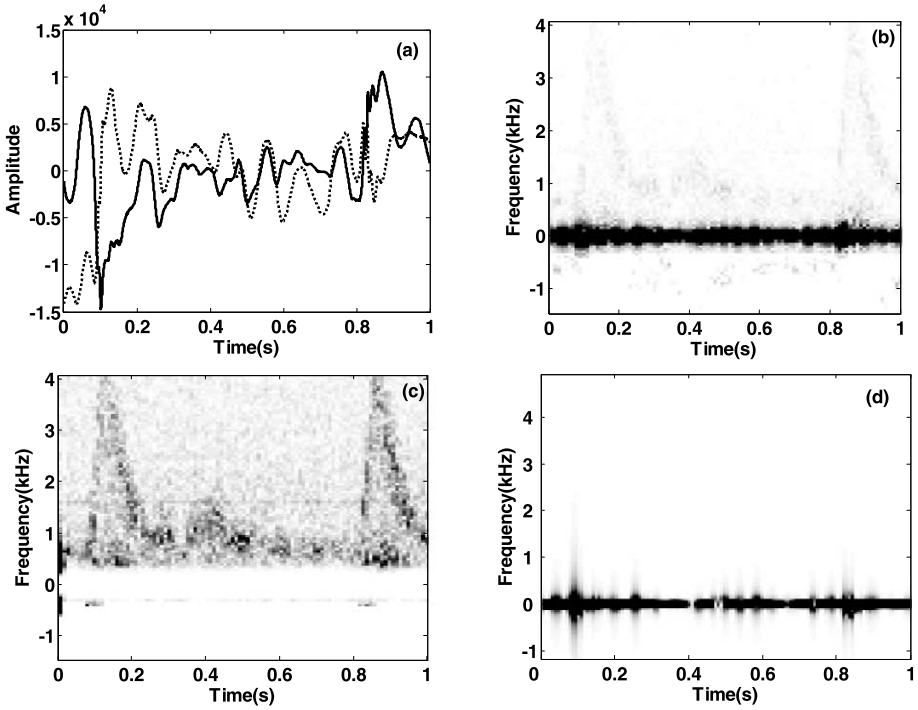

Fig. 8. The in-phase (solid curves) and quadrature (dashed curves) time-domain waveforms (a) of a real I/Q compound signal obtained from the carotid artery with an approximate 10% stenosis degree, the STFT-based compound-spectrogram (b), the blood flow- (c) and wall-spectrograms (d) separated by using a HPF with 400 Hz cutoff frequency.

change from lamina to turbulence with the raise of the stenosis degrees in the stenosed vessels due to the disturbance of the atherosclerotic plaque. These results are coincided with clinical findings of vortices or turbulence in stenosed carotid arteries [7]. The STFT-based spectrograms of the simulated axial (Fig. 4(m)–(o)) and radial (Fig. 5(m)–(o)) blood flow signals, and pulsatile vessel wall signals (Fig. 6(c)), as well as the compound Doppler signals (Fig. 7(g)–(i)) suggest the similarities between the simulated and corresponding theoretical versions. Moreover, obvious random Doppler speckles appear on these STFT-based spectrograms of the simulated signals also resemble the observation in the clinical ones. These results provide valuable visual-comparisons for demonstrating the validation of the proposed simulation method. Furthermore, the validation of the simulation method reported in this study is quantitatively demonstrated by the small MSDs of NRMSESs between the theoretical and averaged STFT-based spectrograms of mixed signals for the stenosis grades of 0%, 10% and 25% over the 30 realizations. It is worth noting that the proposed method is used to simulate a continuous wave (CW) Doppler ultrasound system, which receives compound Doppler signals scattered from the pulsatile blood flow and stenosed common carotid arteries in view of the determined sample volume. However, the cosine-superposed method denoted in Eq. (11) is unsuitable for the simulation of a pulse wave (PW) system due to its small duration and sample volume leading to the non-Rayleigh amplitudes distributions of the received signals. To simulate the real PW Doppler system, the radio frequency echo signals of the moving scatterers in the entire arterial lumen with axial and radial velocity profiles determined by Eq. (6) could be firstly achieved by employing FIELD II software proposed by Jensen [30]. Then the radio frequency echo signals during a specific range locating at a transmission axial-position from the face of the transducer are selected and demodulated to produce the envelops to achieve the corresponding pulse

wave Doppler signals. Another limitation to this simulation method is embodied in the assumption of the movement independence between the blood flow and arterial walls, which does not completely describe the influence on the blood flow profile by the elastic vessel wall. By considering the physiologically cyclic interactions between the blood flow and stenosed vessel walls, future work could be implemented for improving the performance of the presented simulation method to obtain more desirable results.

6. Conclusions

A computer simulation method is presented to produce compound Doppler ultrasound signals scattered simultaneously from both blood flow and vessel wall of pulsatile common carotid arteries with a stenosis. To simulate the I/Q blood flow signals, the axial and radial velocity profiles of pulsatile blood flow are firstly obtained by solving the NSEs in view of the center velocity of a normal vessel and geometric characteristics of the stenosed vessel, and then, the signals are simulated by superposing a series of cosine functions regulated by the spectrograms estimated from the axial and radial velocity profiles, respectively. Meanwhile, the I/Q Doppler signals echoed from pulsatile near and far walls are simulated based on their wall radial movements during a cardiac cycle. Ultimately, the confirmed quadrature signals incorporating the moving information backscattered from both axial and radial flows as well as pulsatile vessel walls are summed to generate the compound Doppler signals with regard to a definite sample volume. The simulator competency to generate the compound Doppler signals with the features resembled to those obtained in clinic has been illustrated in the experimental results. It can be concluded that the proposed computer simulation method can produce compound Doppler signals with confirmed qualitative and quantitative characteristics resembled with the clinical versions, which could be used as an theoretical data source for evaluating the performance of the signal separation between pulsatile blood flows and vessel walls with mild stenosed-lesions.

Acknowledgements

This work was supported by the Grant (61261007), (61361010), (61561049) from the National Natural Science Foundation of China and the Grant (2013FA008) from the Key Program of Yunnan Natural Science Foundation.

Conflict of interest

The authors have no conflict of interest to report.

References

[1] T. Dahl, J. Bang, A. Ushakova, S. Lydersen and H.O. Myhre, Parameters describing motion in carotid artery plaques from ultrasound examination: A reproducibility study, *Ultrasound Med. Biol.* **30**(9) (2004), 1133–1143. doi:10.1016/j.ultrasmedbio.2004.07.002.

[2] S. Nobari, R. Mongrain, R. Leask and R. Cartier, The effect of aortic wall and aortic leaflet stiffening on coronary hemodynamic: A fluid-structure interaction study, *Med. Biol. Eng. Comput.* **51**(8) (2013), 923–936. doi:10.1007/s11517-013-1066-1.

[3] J.M. Romero, R.H. Ackerman, N.A. Dault and M.H. Lev, Noninvasive evaluation of arotid artery stenosis: Indications, strategies, and accuracy, *Neuroimaging Clin. N. Am.* **15**(2) (2005), 351–365. doi:10.1016/j.nic.2005.06.005.
[4] R. Taniguchi, A. Hosaka, T. Miyahara, K. Hoshina, H. Okamoto, K. Shigematsu, T. Miyata, R. Sugiura, A.T. Yokobori Jr. and T. Watanabe, Viscoelastic deterioration of the carotid artery vascular wall is a possible predictor of coronary artery disease, *J. Atheroscler. Thromb.* **22**(4) (2015), 415–423. doi:10.5551/jat.24513.
[5] A.T. Yokobori Jr., M. Owa, M. Ichiki, T. Satoh, Y. Ohtomo, Y. Satoh, S. Ohogoshi, Y. Kinoshita and S. Karino, The analysis and diagnosis of unstable behavior of the blood vessel wall with an aneurysm based on noise science, *J. Atheroscler. Thromb.* **13**(4) (2006), 163–174. doi:10.5551/jat.13.163.
[6] D.H. Evans and W.N. McDicken, *Doppler Ultrasound: Physics, Instrumentation and Signal Processing*, Wiley, Chichester, 2000.
[7] J.W. Hallett, J.L. Mills, J.J. Earnshaw, J.A. Reekers and T.W. Rooke, *Comprehensive Vascular and Endovascular Surgery*, Mosby/Elsevier, USA, 2009.
[8] G. Bambi, T. Morganti, S. Ricci, E. Boni, F. Guidi, C. Palombo and P. Tortoli, A novel ultrasound instrument for investigation of arterial mechanics, *Ultrasonics* **42** (2004), 731–737. doi:10.1016/j.ultras.2003.11.008.
[9] M. Tiziano, R. Stefano, V. Francesca, P. Carlo and T. Piero, Clinical validation of common carotid artery wall distension assessment based on multigate Doppler processing, *Ultrasound Med. Biol.* **31**(7) (2005), 937–945. doi:10.1016/j.ultrasmedbio.2005.04.001.
[10] A. Veneziani and C. Vergara, Flow rate defective boundary conditions in haemodynamics simulations, *Int. J. Numer. Meth. Fluids* **47** (2005), 803–816. doi:10.1002/fld.843.
[11] K. Nam, D. Paeng, M.J. Choi and K.K. Shung, Ultrasonic observation of blood disturbance in a stenosed tube: Effects of flow acceleration and turbulence downstream, *Ultrasound Med. Biol.* **34**(1) (2008), 114–122. doi:10.1016/j.ultrasmedbio.2007.07.009.
[12] M.J. Kim and K. Rhee, Computational analysis of nanoparticle adhesion to endothelium: Effects of kinetic rate constants and wall shear rates, *Med. Biol. Eng. Comput.* **49**(7) (2011), 733–741. doi:10.1007/s11517-011-0735-1.
[13] J.S. Lee and Y.C. Fung, Flow in locally constricted tubes at low Reynolds numbers, *J. Appl. Mech.* **37**(1) (1970), 9–16. doi:10.1115/1.3408496.
[14] A.C.H. Yu and L. Lovstakken, Eigen-based clutter filter design for ultrasound color flow imaging: A review, *IEEE Trans. Ultrason. Ferroelectr. Freq. Control* **57**(5) (2010), 1096–1111. doi:10.1109/TUFFC.2010.1521.
[15] D.K.H. Cheung, H.C.T. Chiu, L. Zhang, C. Hu, K.K. Shung and A.C.H. Yu, Adaptive clutter filter design for micro-ultrasound color flow imaging of small blood vessels, in: *IEEE Ultrasonics Symposium*, 2010, pp. 1206–1209.
[16] A.C.H. Yu and R.S.C. Cobbold, Single-ensemble-based eigen-processing methods for color flow imaging – Part I. The Hankel-SVD filter, *IEEE Trans. Ultrason. Ferroelectr. Freq. Control* **55**(3) (2008), 559–572. doi:10.1109/TUFFC.2008.682.
[17] W. You and Y. Wang, A single-ensemble clutter rejection method based on the analytic geometry for ultrasound color flow imaging, *Ultrasound Med. Biol.* **37**(11) (2011), 1909–1922. doi:10.1016/j.ultrasmedbio.2011.07.005.
[18] P. Li, G. Yu, P. Xin and Z. Bian, A clutter removal method for the Doppler ultrasound signal based on a nonlinear diffusion equation, *Meas. Sci. Technol.* **19**(5) (2008), 055101.1–055101.13. doi:10.1088/0957-0233/19/5/055101.
[19] Y. Zhang, N. Su, Z. Li, Z. Gou, Q. Chen and Y. Zhang, Assessment of arterial distension based on continuous wave Doppler ultrasound with an improved Hilbert–Huang processing, *IEEE Trans. Ultrason. Ferroelectr. Freq. Control* **57**(1) (2010), 203–213. doi:10.1109/TUFFC.2010.1399.
[20] Y. Zhang, Y. Gao, L. Wang, J. Chen and X. Shi, The removal of wall components in Doppler ultrasound signals by using the empirical mode decomposition algorithm, *IEEE Trans. Biomed. Eng.* **54**(9) (2007), 1631–1642. doi:10.1109/TBME.2007.891936.
[21] Q. Tao, Y. Wang, C. Jose and W. Wang, Simulating Doppler ultrasound blood flow signals with the pulsation of the vascular wall, *Acta Acustica (Chinese version)* **29**(3) (2004), 267–271.
[22] Y. Zhang, J.C. Cardoso, Y. Wang, P.J. Fish, C.A.C. Bastos and W. Wang, Time-scale removal of "wall thump" in Doppler ultrasound signals: A simulation study, *IEEE Trans. Ultrason. Ferroelectr. Freq. Control* **51**(9) (2004), 1187–1192. doi:10.1109/TUFFC.2004.1334852.
[23] Q. Tao, Y. Wang, P. Fish, W. Wang and J. Cardoso, The wall signal removal in Doppler ultrasound systems based on recursive PCA, *Ultrasound Med. Biol.* **30**(3) (2004), 369–379. doi:10.1016/j.ultrasmedbio.2003.11.014.
[24] Y. Zhang, Y. Wang, W. Wang and B. Liu, Doppler ultrasound signal denoising based on wavelet frames, *IEEE Trans. Ultrason. Ferroelectr. Freq. Control* **48**(3) (2001), 709–716. doi:10.1109/58.920698.
[25] P.J. Fish, C.A.C. Bastos and F. Vaz, Blood and wall signal simulator for Doppler ultrasound signal analysis algorithm development, in: *Proc. 23rd Annual EMBS International Conference*, Vol. 1, Istanbul, Turkey, 2001, pp. 135–138.
[26] L. Gao, Y. Zhang, K. Zhang, G. Cai, J. Zhang and X. Shi, A computer simulation model for Doppler ultrasound signals from pulsatile blood flow in stenosed vessels, *Comput. Biol. Med.* **42**(9) (2012), 906–914. doi:10.1016/j.compbiomed.2012.07.002.

[27] Y. Zhang, L. Gao, K. Shen, K. Zhang, J. Yan, W. Cheng and J. Zhang, A simulator for mixed Doppler ultrasound signals from pulsatile blood flow and vessel wall with mild stenosis, in: *Proc. 35rd Annual International Conference of the IEEE EMBS*, Osaka, Japan, 2013, pp. 1903–1906.
[28] Z.Q. Bian and X.G. Zhang, *Pattern Recognition*, Tsinghua University Press, 2000, pp. 1–60.
[29] L.Y.L. Mo and R.S.C. Cobbold, "Speckle" in continuous wave Doppler ultrasound spectra: A simulation study, *IEEE Trans. Ultrason. Ferroelectr. Freq. Control* **33**(6) (1986), 747–753. doi:10.1109/T-UFFC.1986.26891.
[30] J. Jensen, Field: A program for simulating ultrasound systems, *Med. Biol. Eng. Comput.* **34** (1996), 351–353. doi:10.1007/BF02520003.